Chemical Engineering Journal 430 (2022) 132842

Contents lists available at ScienceDirect

Chemical Engineering Journal

journal homepage: www.elsevier.com/locate/cej

A defect-rich layered double hydroxide nanofiber filter with solar-driven regeneration for wastewater treatment

Yibo Dou [a], Yuechao Yao [a], Gege Wu [a], Guohua Gao [b], Martin Zatloukal [c,*], Claus Hélix-Nielsen [a,*], Wenjing Zhang [a,*]

[a] Department of Environmental Engineering, Technical University of Denmark, Miljøvej 113, Kgs. Lyngby 2800, Denmark
[b] Shanghai Key Laboratory of Special Artificial Microstructure, School of Physics Science and Engineering, Tongji University, Shanghai 200092, PR China
[c] Polymer Centre, Faculty of Technology, Tomas Bata University in Zlin, Vavreckova 275, Zlin 760 01, Czech Republic

ARTICLE INFO

Keywords:
Wastewater treatment
Defect-rich layered double hydroxide
Solar-driven regeneration
3D filter modelling simulation
Contaminants of emerging concerns

ABSTRACT

The need for environmental technology treatment of contaminants of emerging concerns (CECs) is increasing as CECs lead to detrimental effects on human health and ecosystems. Herein, defect-rich layered double hydroxide (LDH) structured into a fibrous filter with a facile solar-driven regeneration function was fabricated for efficiently removing adsorbed CECs in wastewater. The physical and chemical interactions between the LDH filter and CECs are revealed. It is demonstrated that the introduction of unsaturated $Cu^{\delta+}$ sites ($\delta < 2$) and creating oxygen vacancies represents an effective way for improving adsorbing activity of the defect-rich LDH host layer. Also, the nanofiber-particle friction coefficient of the hierarchical LDH filter affects the filtration efficiency as revealed by 3D modelling. The LDH filter is capable of filtrating sixteen types of CECs and shows the capability of photocatalytic degradation of adsorbed CECs, thus enabling filter regeneration. This work thus presents a new perspective into bottom-up design of adsorbent materials: from molecular interactions to shaping adsorbents into microscopic nanofibers and assembling these into macroscopic 3D adsorbent filters.

1. Introduction

With the ever-increasing population growth and advancements in medical treatments and industrial processes, a growing number of contaminants are entering the aqueous environment from human activity [1–3]. In particular, for industrialized countries, the concerns for public health and environmental impact are exemplified by the widespread use of pharmaceuticals and their significance as contaminants of emerging concerns (CECs) [4,5]. Low-molecular-weight CECs penetrate barriers in conventional wastewater treatment plants and enter the aqueous environment. Highly persistent CECs, such as antibiotics ciprofloxacin and erythromycin, blood pressure regulators hydrochlorothiazide (HCT) and atenolol, analgesics carbamazepine, antidepressants sertraline may lead to detrimental effects on the survival and growth of aquatic organisms, even at low concentrations [4]. Especially, extended exposure to CECs residues in the environment may enrich antibiotic-resistant genes [6]. Thus, there is an urgent need for a sustainable and effective wastewater treatment technology. Among various developed strategies, adsorption processes are widely applied because of their easy operation, low energy consumption and relatively low cost. However, there are still challenges limiting applications [7–9]. For example, most developed adsorbents are in the form of powders, which may promote adsorbent agglomeration, thus reducing capacity and kinetics [10,11]. Moreover, there is a general issue in separating adsorbent powder from treated water. When the adsorbents are saturated with contaminants, regeneration typically requires washing with water or organic solvent, with potential risks of secondary contamination [12]. In particular, some captured contaminants have a strong affinity to the adsorbents, leading to inefficient regeneration. In most cases, the adsorbents are simply discarded or incinerated after use, which in itself presents a major sustainability challenge.

To tackle these issues, structuring of absorbents in the form of coatings, membranes, or devices may present a strategy for creating a material with high removal capability and which meets practical application requirements [13–15]. In principle, electrospinning technology, in which adsorbents are structured into various nonwoven nanofibers (NFs), can enable a low-pressure combined absorption-filtration process for environmental remediation. However, fibrous

* Corresponding authors.
E-mail addresses: mzatloukal@utb.cz (M. Zatloukal), clhe@env.dtu.dk (C. Hélix-Nielsen), wenz@env.dtu.dk (W. Zhang).

https://doi.org/10.1016/j.cej.2021.132842
Received 28 July 2021; Received in revised form 29 September 2021; Accepted 1 October 2021
Available online 16 October 2021

filters which integrate porous adsorbents into a polymer matrix can result in densification or blockage of pores, causing the loss of active sites and decreased filtration efficiency [16,17]. Also, the filtration behavior is not merely dependent on the intrinsic adsorbent efficacy on NFs, but also depends on the morphology and surface roughness induced friction between NFs and contaminates, as well as external factors such as transmembrane pressure and cross-flow rates.

Layered double hydroxides (LDHs) are one class of host–guest materials, which have a general formula of $[M^{2+}_{1-x}M^{3+}_{x}(OH)_2]^{x+}$ $(A^{n-})_{x/n}\cdot yH_2O$. The host 2D layers was constructed by edge-shared metal M(II) and M(III) hydroxide octahedral, and the interlyaer is filled with neutralized anions [18,19]. The LDHs normally show cost-effective, environmentally friendly, special ion exchange and structural memory properties. As a resut, the LDH based functional materials have been widely used in catalysis, gas barrier, adsorbents, and biology. Especially, LDHs have been reported for adsorption of various contaminants, owing to their large surface area, tunable chemical composition and special ion exchange capability [18–21]. However, the adsorption performance of LDH normally in the form of bulk powder is limited by insufficient adsorption capacity and poor regeneration performance. Here we designed LDH-based NFs as a filter with solar-driven regeneration capability for treating wastewater with CECs (Scheme 1). To enrich active sites of LDHs for maximizing adsorption capacity, we propose a defect engineering strategy by creating unsaturated $Cu^{\delta+}$ sites and oxygen vacancy (V_O) on LDH cationic layers which are structured into fibrous filters. Filtrations combined with 3D modelling simulation were performed to demonstrate the high removal efficiency compared to other adsorbent filters. In addition, the photocatalytic property of the LDH filter was investigated to demonstrate how filters can be easily regenerated.

2. Results and discussion

2.1. Fabrication and characterization of CoNiCu-LDH NFs

PAN@AlOOH@LDH NFs denoted as LDH NFs are fabricated as follows, see Fig. 1a (for details, please refer to the experimental section). Firstly, the polyacrylonitrile (PAN) NFs are fabricated by the electrospinning method (Fig. S1a), for use as a flexible substrate for constructing 3D filters. Then, an aluminum oxihydroxide boehmite (AlOOH) gel is dip-coated on PAN NFs to obtain AlOOH NFs (Fig. S1b). The presence of AlOOH coating protects the inner polymer PAN NFs and improves interfacial compatibility. Subsequently, Co-containing zeolitic imidazolate framework with a leaf-like morphology (Co-ZIF-L) as a template is grown on the surface of AlOOH NFs to fabricate ZIF-L NFs (Fig. S2). Finally, CoNiCu-LDH NFs are fabricated by ion-exchange on ZIF-L NFs. The resultant flexible LDH NFs mat has a sea-green colour, and scanning electron microscopy (SEM) micrographs showed a honeycomb-like structure on the surface of the AlOOH NFs (Fig. 1b-c). The hierarchical (Fig. 1d) and porous structure (Fig. 1d, inset) were revealed by transmission electron microscopy (TEM). The TEM image showed a lattice spacing of 0.26 nm (Fig. 1e), which is attributed to the (0 1 2) crystal plane of the LDH. In addition, the energy-dispersive X-ray spectroscopy (EDX) mapping showed CoNiCu-LDH NFs with a homogeneous element distribution (Fig. 1f). The molar ratio for Co: Ni : Cu: is around 4.5 : 4.1 : 1.3 (Fig. S3). The X-ray diffraction (XRD) confirmed the structural conversion process from Co-ZIF-L to CoNiCu-LDH (Fig. 1g and S2a). Based on the LDH synthesized by previous reported hydrothermal and separate nucleation and aging steps (SNAS) methods, [22,23] the low intensity of XRD peak observed here can be attributed to defects on the host layer of LDH created by the introduction of Cu sites giving rise to a Jahn-Teller effect [24,25]. The electronic structure of CoNiCu-LDH NFs was investigated by X-ray photoelectron spectroscopy (XPS). Compared with CoNi-LDH NFs, the binding energy of Ni 2p and Co 2p of CoNiCu-LDH NFs leads to a positive shift, implying a modified local electronic density of Ni and Co sites on the cationic layer (Fig. 1h-i). Meanwhile, the O 1 s peak of the CoNiCu-LDH NFs shifted to higher binding energy than CoNi-LDH (Fig. 1j), and a new peak located at 533.8 eV probably reflects a high number of V_O [26]. The result thus indicated that the introduction of Cu modified the electronic microenvironment and created V_O on the defective LDH layer.

2.2. The adsorption behavior investigation of LDH NFs as adsorbent

Before the LDH NFs were structured into a 3D filter, we evaluated their adsorption performance. As an exemplary CEC, we use the blood pressure regulator hydrochlorothiazide (HCT) as model adsorbate. Fig. 2a shows the adsorption concentration (q_t) as a function of adsorption time for various NFs. The CoNiCu-LDH NFs exhibited higher adsorption capacity (317 mg g^{-1}) than CoNi-LDH NFs (299 mg g^{-1}). The

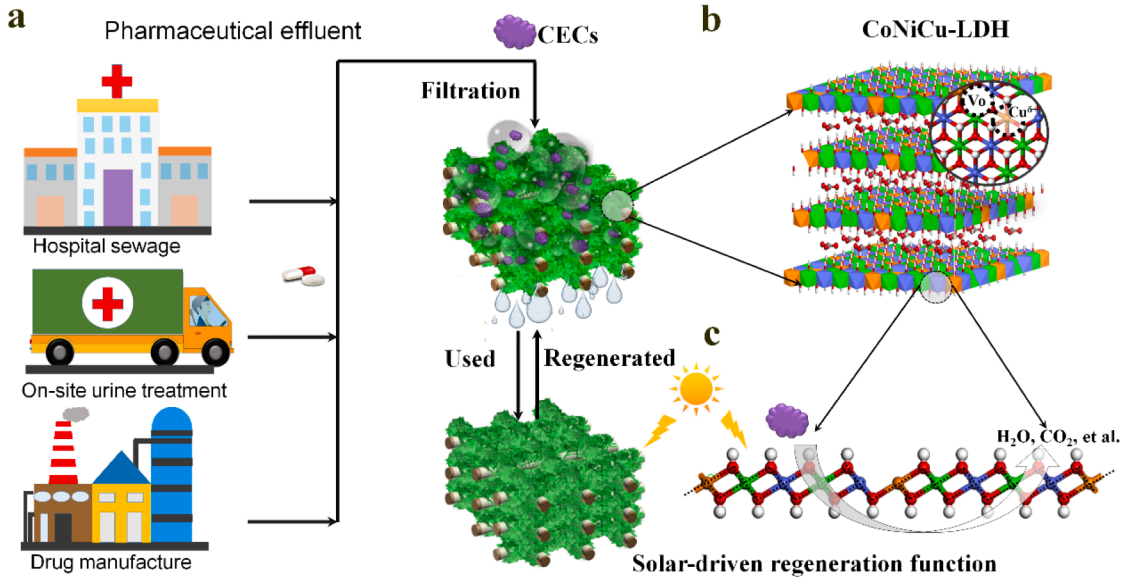

Scheme 1. (a) LDH with enriched defects sites that structured into NFs filter with solar-driven regeneration function for the removal of CECs. (b) The structure of CoNiCu-LDH, with unsaturated $Cu^{\delta+}$ and V_O on the LDH slab. (c) The solar-driven regeneration mechanism of the LDH filter via photocatalytic degradation of adsorbed CECs.

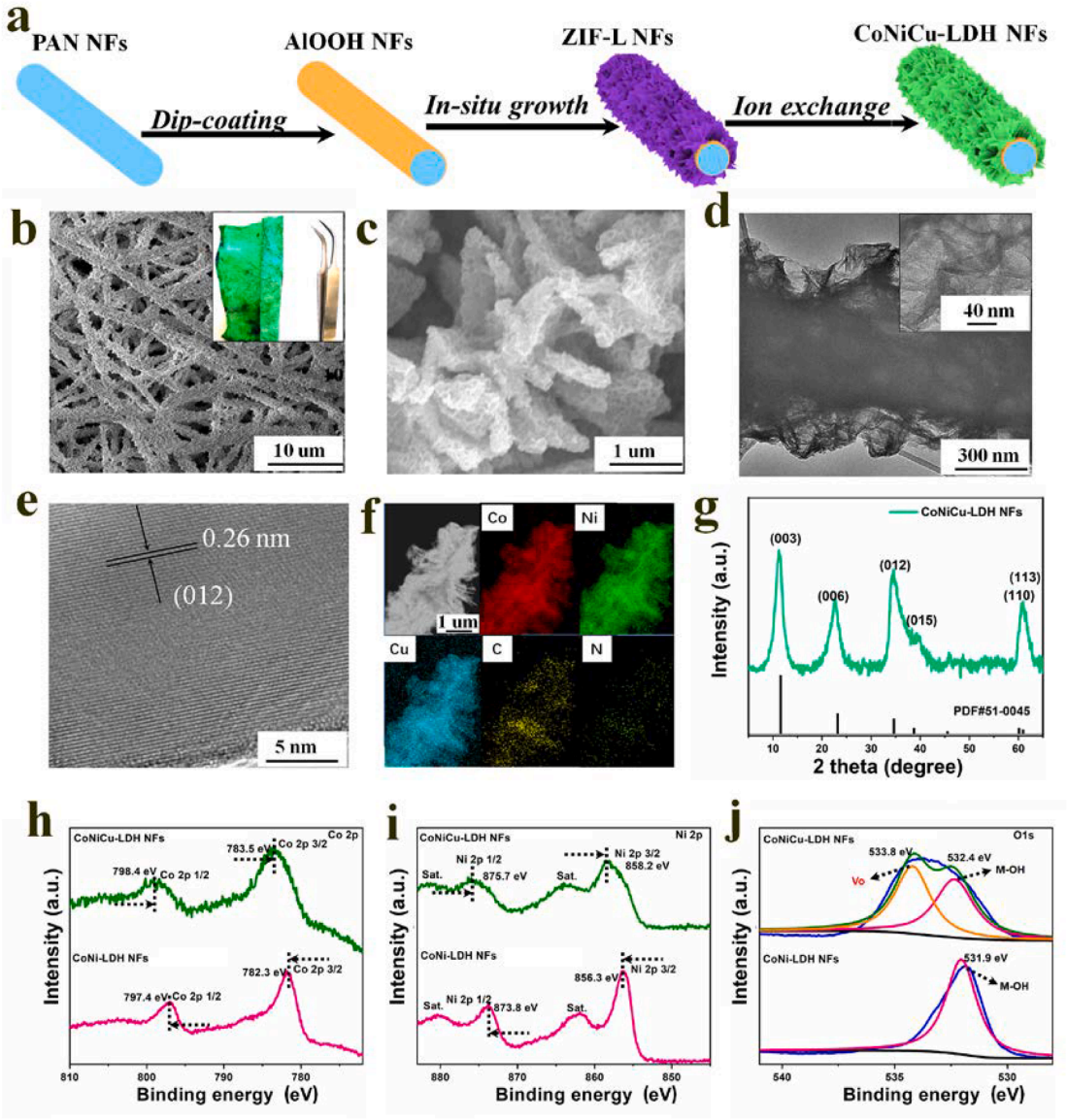

Fig. 1. (a) Schematic illustration for the fabrication of the CoNiCu-LDH NFs. (b) Low and (c) high magnification SEM images, (d) low and (e) high magnification TEM images, (f) EDX mapping and (g) XRD pattern for the CoNiCu-LDH NFs. XPS spectra of (h) Co 2p, (i) Ni 2p and (j) O 1 s for CoNiCu-LDH NFs and CoNi-LDH NFs, respectively.

PAN NFs and AlOOH NFs have negligible adsorption capacity, indicating LDH plays a crucial role in capturing HCT molecules. The adsorption equilibrium time is reached within 10 min. The fast initial adsorption rate can be attributed to readily accessible sites enabled by the hierarchically super-hydrophilic fibrous structure (Fig. S4). Thus, the result indicates that the adsorption process is controlled by external mass transfer instead of intra-particle diffusion mass transfer.[27,28] The reason is probably because of the honeycomb-like structure of LDH, which exposed active sites to the external surface. Most importantly, the CoNiCu-LDH NFs showed higher adsorption capacity than that of CoNi-LDH NFs for absorbing other two blood pressure regulators: atenolol and sulfamethoxazole (Fig. 2b and S5). The above results indicated the introduction of Cu site in the LDH slab leads to more active sites for promoting adsorption.

Moreover, the HCT adsorption isotherms for CoNiCu-LDH NFs were obtained. The values of equilibrium concentration (q_e) increased with increasing HCT concentration (c_e) initially and gradually became stable (Fig. 2c). Langmuir and Freundlich models were applied to analyze the adsorption behavior.[27,28] The results indicated that the adsorption curve for CoNiCu-LDH NFs fits the Langmuir model for Ce > 100 mg L^{-1} and the Freundlich model for Ce < 100 mg L^{-1} (Fig. S6). This result illustrates that the adsorption was not limited to the formation of monolayer coverage of adsorbate on a homogeneous LDH surface, probably because of abundant and different adsorption sites. Furthermore, the calculated Gibbs free energy change (ΔG) of –0.150 kJ mol^{-1} revealed that the adsorption process was spontaneous under standard conditions [27].

To compare CoNiCu-LDH NFs with other LDH-based NFs, we synthesized MgAl-LDH NFs and CoAl-LDH NFs (Fig. S7 and S8) previously reported in the literature [29]. The adsorption capacities of the three adsorbents followed the order CoNiCu-LDH NFs (317 mg g^{-1}) > MgAl-LDH NFs (223 mg g^{-1}) > CoAl-LDH NFs (160 mg g^{-1}) (Fig. 2d), showing the composition on LDH host layer affects the adsorption capacity. Moreover, the honeycomb-like CoNiCu-LDH on the polymer NFs exhibited the highest surface area with 407 cm^3 g^{-1} compared to MgAl-LDH NFs (213 cm^3 g^{-1}) and CoAl-LDH NFs (91 cm^3 g^{-1}) (Fig. 2e). Thus, the results illustrated the higher adsorption capacity of the defect-rich CoNiCu-LDH can be attributed to the high surface area and introduced

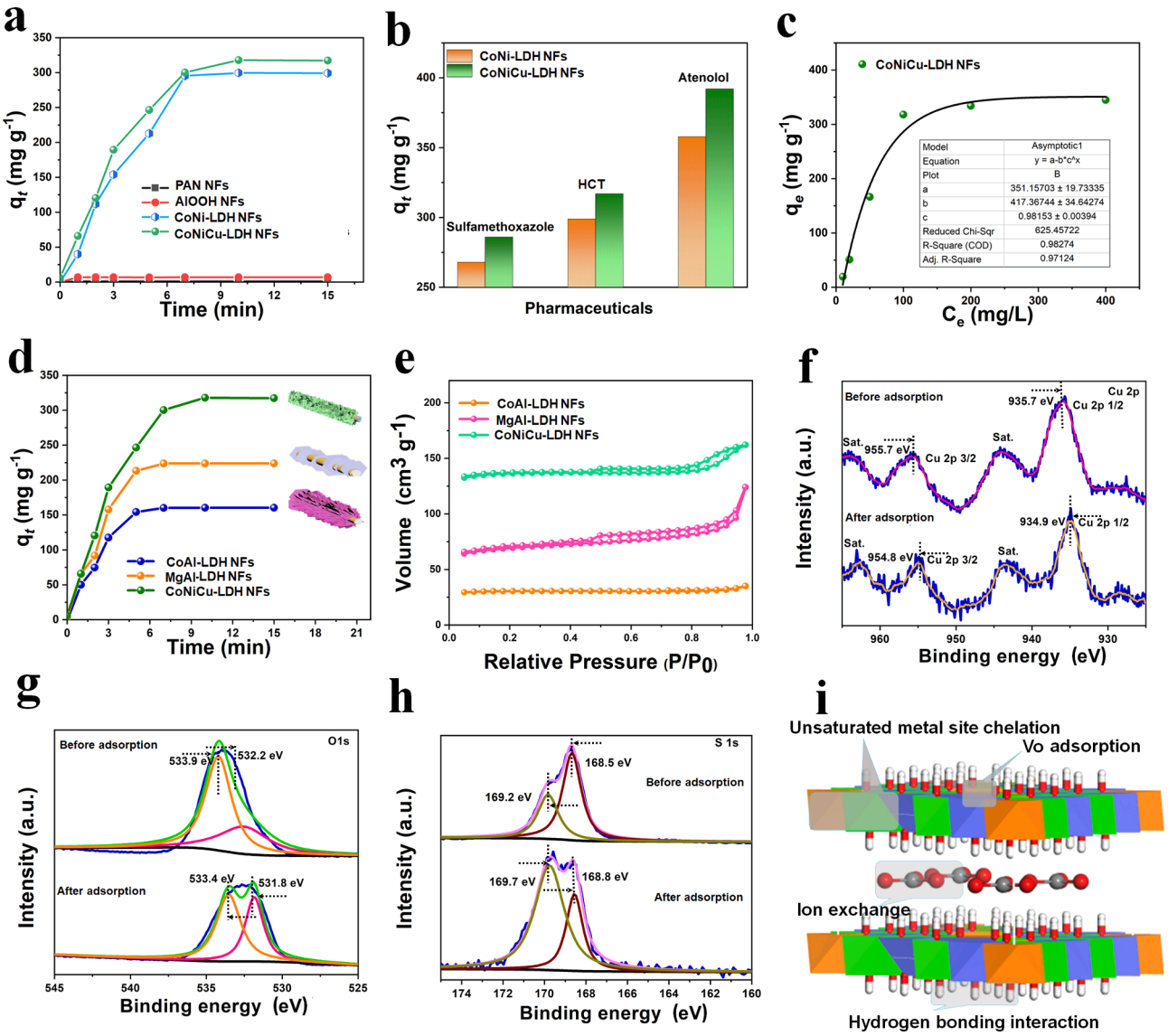

Fig. 2. (a) The HCT adsorption curves as the function of time on various fibrous adsorbents that PAN, AlOOH, CoNi-LDH, CoNiCu-LDH NFs, respectively. (b) The q_t of CoNi-LDH and CoNiCu-LDH NFs on absorbing HCT, atenolol and sulfamethoxazole, respectively. (c) The adsorption isotherms of HCT onto the CoNiCu-LDH NFs. (d) The HCT adsorption curves as the function of the time and (e) N_2 adsorption/desorption isotherm curves for MgAl-LDH, CoAl-LDH, CoNiCu-LDH NFs with different morphology. (f) Cu 2p and (g) O 1 s XPS spectra of adsorbent CoNiCu-LDH NFs as well as (h) S 1 s XPS spectra of adsorbate HCT before and after adsorption, respectively. (i) The proposed adsorption mechanism for CoNiCu-LDH NFs.

Cu sites on LDH host layer.

To identify the active adsorption sites, we used XPS to measure the shift in binding energy for the elements in CoNiCu-LDH NFs before and after adsorption. Adsorption of HCT resulted in an apparent negative binding energy shift of 0.9 eV for Cu $2p_{3/2}$ and 0.8 eV for Cu $2p_{1/2}$ (Fig. 2f). The result indicated that Cu sites are more active on LDH host layer for HCT adsorption. In addition, the O 1 s spectra displayed a negative shift of 0.5 and 0.6 eV (Fig. 2g), indicating the adsorbate interacted with the V_o and hydroxyl group on the LDH host layer. The binding energy of S 1 s for the HCT absorbed on NiCoCu-LDH NFs exhibited a positive shift compared with that of pure HCT (Fig. 2h). The decreased binding energy of O 1 s on LDH and the increased binding energy of S 1 s on HCT indicated the occurrence of charge transfer from HCT to CoNiCu-LDH during the adsorption process [30]. Based on these results, we propose that there are four possible active adsorption pathways: unsaturated metal site chelation, V_o adsorption, interlayer ion exchange and hydrogen bonding (Fig. 2i). In contrast to other types of LDH, electron-rich V_o and unsaturated $Cu^{\delta+}$ ($\delta < 2$) sites existed in the defect-rich CoNi-LDH, both of which may interact with the amino group of HTC. The results indicated that creating V_o and introducing unsaturated metal sites is a feasible strategy to improve the adsorption capability of the LDH-based adsorbent.

2.3. The evaluation of the filtration performance of LDH filters

The LDH NFs was then constructed into a three-dimensional (3D) filter by cutting LDH NF mats into disks which were stacked layer-by-layer and compressed to obtain a dense 3D fibrous filter (Fig. 3a). The resulting LDH filter was first used to filtrate the 100 mg L^{-1} HCT solution under various flow rates. For flow rates up to 10 ml cm^{-3} min^{-1}, the filtration efficiency of LDH NFs was relatively low (<50%) due to the short retention time providing insufficient interaction between HCT and the CoNiCu-LDH in the NF filter (Fig. 3b). In comparison, when the flow rate was reduced to 4 ml cm^{-3} min^{-1}, the removal efficiency of HCT reached 85% for at least 140 min.

To investigate the filtration process in detail, we used our developed

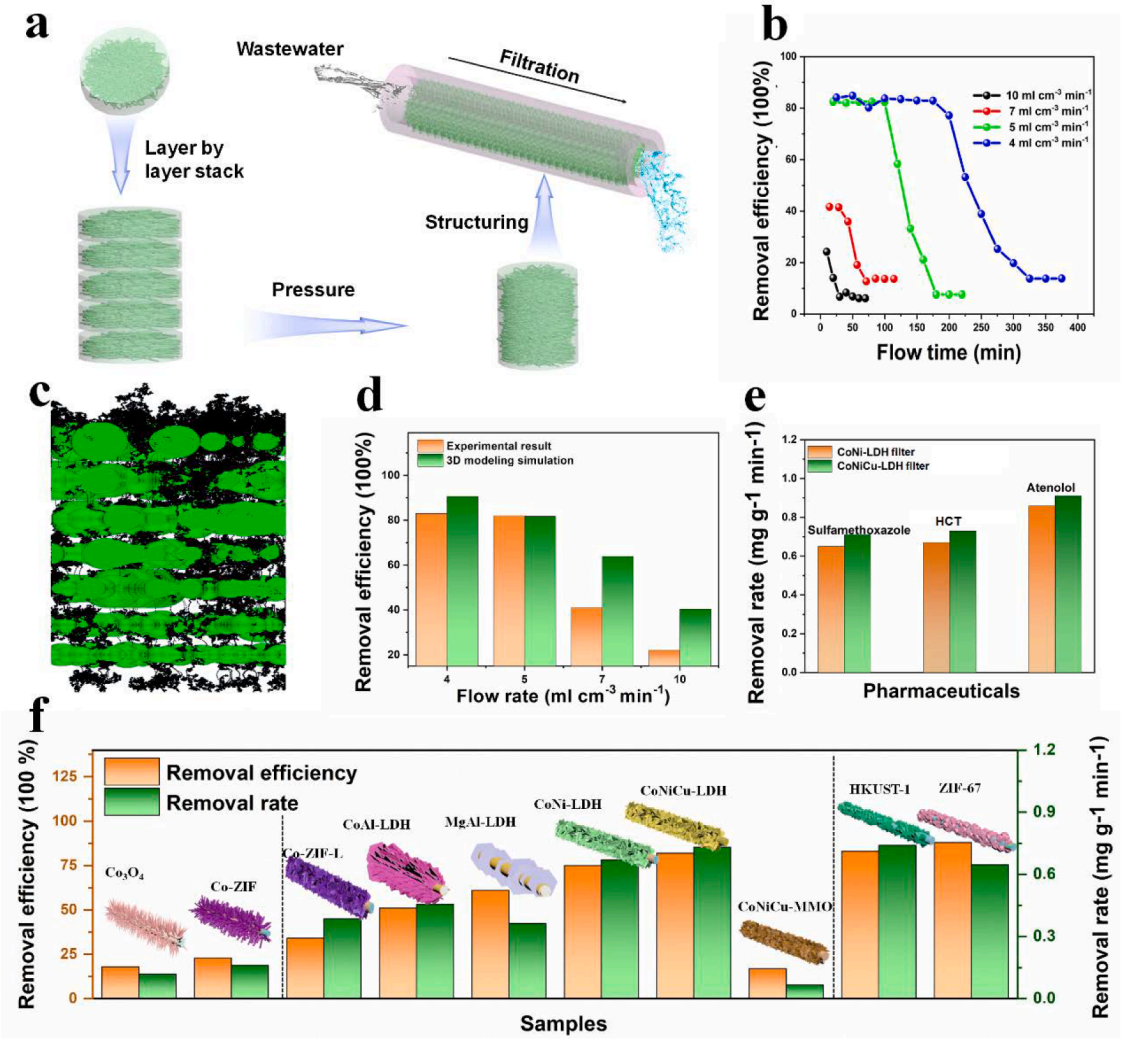

Fig. 3. (a) Schematic illustration for shaping the CoNiCu-LDH NFs into filter for the removal of CECs. (b) The removal efficiency of the CoNiCu-LDH filter as a function of time under various flow rates. (c) The simulated 3D structured CoNiCu-LDH filter for HCT filtration. (d) The simulated and experimental removal efficiency for the CoNiCu-LDH filter under various flow rates. (e) The removal efficiency for the CoNiCu-LDH and CoNi-LDH filters as a function of time at a flow rate of 5 ml cm^{-3} min^{-1}. (f) The proposed general methodology for structuring 1D Co_3O_4 and Co-ZIF nanorod, 2D Co-ZIF-L, CoAl-LDH, MgAl-LDH, CoNi-LDH, CoNiCu-LDH and CoNiCu-MMO, 3D HKUST-1 and ZIF-67 into filters, and their removal efficiency and the removal rate, respectively.

software to solve the Langevin equation with the Stokes' law drag force by the Lagrangian method to model the 3D Brownian motion of each molecule suspended in a one direction flowing water through the constructed 3D nanofiber filter model [31,32]. The use of the chosen simulation strategy is justified by the creeping flow conditions occurring during the performed filtration experiments [33], because the Reynolds numbers for the flow of water through the filter nanopores are much<0.1. The adsorption or slippage of the molecule on the surface of the fiber was determined based on the force balance considering drag force, lift force, adhesion (van der Waals) force and the friction force. A similar modeling strategy has already been successfully used in our previous work for modeling air filtration using polyurethane nanofiber filters, which also meets the conditions for the creeping flow [31,32]. The filtration efficiency for HCT was simulated in the constructed LDH filter model at different flow rates (details of the simulation process can be found in the Supporting Information). The comparison showed that the 3D simulated filtration efficiency exhibited a similar trend as the experimental results (Fig. 3d), where a decrease in the flow rate improved the filtration efficiency. The flow rate of 5 ml cm^{-3} min^{-1} is confirmed as an optimized flow rate where CoNiCu-LDH NFs achieved a maximum removal rate of 0.73 mg g^{-1} min^{-1} (Fig. S9). Even though CoNiCu-LDH NFs showed the highest removal efficiency, the removal rate was only 0.58 mg g^{-1} min^{-1} with a flow rate of 4 ml cm^{-3} min^{-1}. Moreover, the CoNiCu-LDH NFs filter showed a higher removal rate than the NiCo-LDH NFs filter (Fig. 3e), due to the active Cu sites (Fig. 2h). This phenomenon was confirmed via filtration of atenolol and sulfamethoxazole (Fig. S10).

Based on the CECs filtrations, we conclude that the proposed synthesis and structuring strategy to structure adsorbent into hierarchical NFs would provide not only active sites for adsorption but also endow free space among NFs to facilitate mass transfer, leading to a fast and efficient filtration performance. To prove this universal methodology for fabricating adsorbents filter, we structured a series of adsorbents, including metal oxides, LDHs and metal–organic frameworks (MOFs), into NF filters (Fig. 3f, S11, and S12). As for the NF filters decorated with 1D nanorods, such as Co_3O_4 filter and Co-ZIF filter, both removal efficiency and removal rate are relatively low. In comparison, the adsorbents Co-ZIF-L and CoNiCu-LDH filter show higher filtration performance as the 2D surface allows for a higher density of active sites [34]. The LDH converted porous mix metal oxide (MMO) have been reported to have high adsorption capacity [28]. However, the filtration performance of the CoNiCu-MMO filter derived from the CoNiCu-LDH filter via calcination is low as pyrolysis process damaged the MMO NFs structure (Fig. S12f). Moreover, two MOFs, which have been

recently reported as excellent adsorbents, were structured into NF filters for comparison as well. Owing to the microporous structure of MOF adsorbents, the 3D ZIF-67 and HKUST-1 filter exhibit comparable filtration performance with that of the CoNiCu-LDH NFs. Nevertheless, the poor chemical and thermal stability of MOF adsorbents are among the major challenges limiting practical applications in chemically harsh wastewater environments [35]. The above result thus demonstrated that our developed general methodology is effective for fabricating adsorbents filter with high and stable efficiency.

2.4. The generality and selectivity of LDH filter for removal of CECs

In view of the advantages of the CoNiCu-LDH filter discussed above, we then used it to remove various potential CECs, including antibiotics, analgesics, antidepressants, X-ray contrasts, immunosuppressant, anti-inflammatory anti-corrosion, herbicides, blood pressure regulators and lipid-lowering agents. As shown in Fig. 4a and 4b, the CoNiCu-LDH filter with abundant active sites can be used to remove sixteen selected CECs. The CoNiCu-LDH filter also showed filtration selectivity of various CECs (Fig. S13). In particular, the results show that the adsorption and filtration behavior is not solely dependent on the chemical interaction of pristine LDH adsorbent with CECs but also related to the structure of the NF filter. To investigate this in more detail we propose the following phenomenological equation to describe the effects of particle-fiber friction and chemical interactions on the filtration efficiency:

$$\xi = \frac{1}{2}\xi_0\left[\left(\frac{D_{AverageMaxFiberDiameter}}{D_{AverageMinFiberDiameter}}\right)^2 + \left(\frac{D_{AverageFiberDiameter}}{D_{ParticleDiameter}}\right)^N\right] \quad (1)$$

where ξ is the total particle-fiber friction coefficient, ξ_0 is the "interaction-free" friction coefficient, and N is the chemical interaction parameter. In the absence of surface roughness (meaning the average maximum NF diameter $D_{AverageMaxFiberDiameter}$ is equal to average minimum NF diameter $D_{AverageMinFiberDiameter}$) and chemical interactions between the particle ($N = 0$), both terms in the square brackets will be unity and ξ will be equal to ξ_0. The chemical interaction parameter N for a given absorbance particle was determined from filtration experiments (blue lines in Tables S2 and S3) to match the experimentally measured filtration efficiency data at a given volume flow rate. First, without considering the impact of chemical interactions, we can see from Fig. 4c that the filtration efficiency increases with the NF frictions. Second, $N = 1.5$ for HCT and 2.6 for erythromycin was obtained based on equation (1) (see detail in Supporting Information), indicating the chemical interaction also existed between LDH and these CECs during the filtration process. The reason that HCT-NFs has smaller N value as compared with erythromycin-NFs is that the Brownian motion effect is stronger for the smaller HCT compared to the larger erythromycin. Thus, the measured higher filtration efficiency for erythromycin can be explained by a higher chemical activity with $N = 2.6$ due to hydroxyl groups interacting with the LDH filter.

As for the selective adsorption capacity, the activity of CoNiCu-LDH NFs depends on functional groups of CECs. The five blood pressure regulators with similar size and structure exhibited the following order of adsorption capacity: bezafibrate > metoprolol > atenolol > HCT > sulfamethoxazole. The reason is that these blood pressure regulators have different function groups to interact with LDH. The high interacting behavior of the function group for CECs normally showed the following order that –COOH (bezafibrate) > –OH (metoprolol, atenolol) > $–NH_2$ (atenolol, HCT, sulfamethoxazole) group, probably because that both host layer –OH group and interlayer anion prone to interact with –COOH. Moreover, the positive active $Cu^{\delta+}$ sites on the alkaline layer would prefer interacting with charged $–COO^-$ group.

Nevertheless, high adsorption capacity does not always lead to high filtration efficiency. When comparing the five blood pressure regulators, removal efficiencies of atenolol and metoprolol are higher, which shows that the filtration behavior is determined not only by the adsorption behavior of LDH, but also is associated with physical particle-fiber friction. In addition, both adsorption capacity and removal efficiency are low for relatively hydrophobic molecules such as carbamazepine, sertraline, clarithromycin. We attributed this to the super-hydrophilic property of LDH NFs (Fig. S4). The results demonstrated that both the hierarchical structure of 3D filter and the interaction between the adsorbent and the CECs molecules play crucial roles in determining the filtration performance.

2.5. Solar-driven regeneration function of the LDH filter

Regeneration and durability are inevitable challenges in wastewater treatment. To regenerate the adsorbent filters, people often apply periodical backflush or chemical cleaning in practical applications, leading

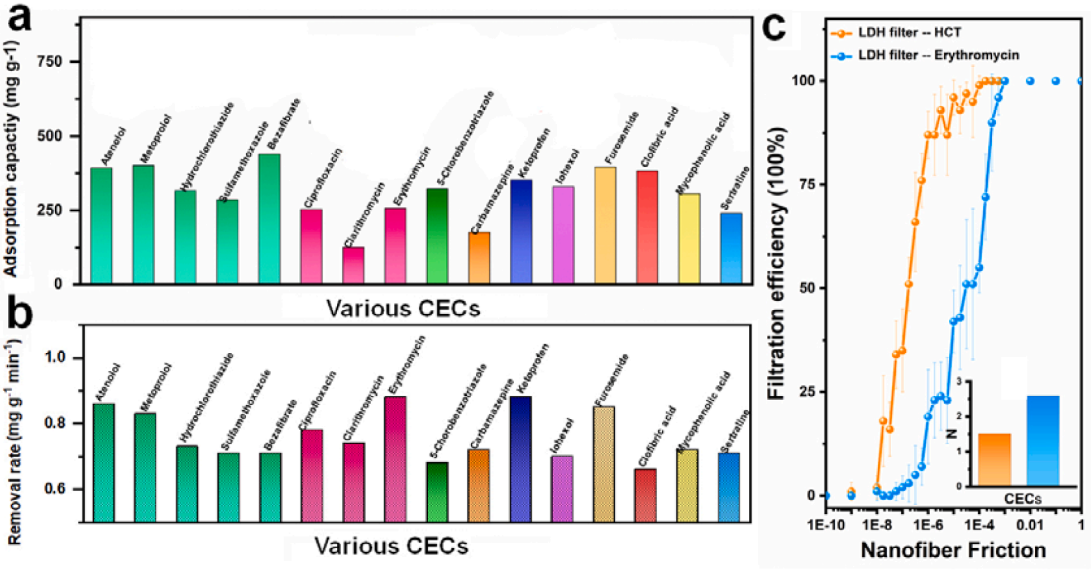

Fig. 4. (a) The adsorption capacity of CoNiCu-LDH NFs and (b) the removal rate of CoNiCu-LDH filter for the removal of sixteen CECs from wastewater (The raw concentration of all CECs solution is 100 mg L^{-1} and the flow rate is 5 ml cm^{-3} min^{-1}). (c) The filtration efficiency of HCT and erythromycin as the function of the fiber friction for CoNiCu-LDH filter during the filtration process.

to not only consumption of water and chemicals, but also to degradation of filter material. Previous work has shown the potential of using LDH for photocatalytic application [24,36]. Our hypothesis is that if the defect-rich CoNiCu-LDH adsorbent has photocatalytic activity, the saturated LDH filter could be regenerated by solar light-driven CEC degradation and reused for circular wastewater treatment process. To verify the hypothesis, we carried out the cycle adsorption tests where the water containing CECs are captured through CoNiCu-LDH filter followed by simulated solar light irradiation. Compared with the saturated CoNiCu-LDH filter without being treated by solar light irradiation (Fig. S14), there was no noticeable loss in the removal efficiency of the CoNiCu-LDH filter after five cycles (Fig. 5a). The obvious decrease of concentration for the CECs solution by using LDH NFs under light irradiation further confirmed the efficient photocatalytic activity of LDH, compared with the blank experiment (Fig. S15). In addition, the CoNiCu-LDH NFs showed higher catalytic activity than that of CoNi-LDH NFs in 1 h. Compared with the traditional regeneration procedure backflush or chemical cleaning, the solar-driven regeneration function is a facile method because of the photocatalytic activities of the LDH-based NFs. It should be noted the degradation of HCT is a combination of UVC alone and action of the photocatalyst. As shown in table S6, the degradation rate constant for HCT in the absence (UVC alone) and presence of the CoNiCu-LDH photocatalyst is 0.009 and 0.028 min^{-1}. The result indicated that some of CECs can be potentially decomposed by solar light irradiation alone, and the introduction of LDH photocatalyst is favorable for improving the degradation kinetics.

To reveal the photocatalysis induced facile regeneration mechanism of NiCoCu-LDH NFs, the specific photocatalytic steps, including light-harvesting, electron-hole separation and surface redox reaction, were investigated [37,38]. As shown in Fig. 5b, the UV–Vis diffuse reflectance spectroscopy illustrated that both CoNi-LDH and defect-rich CoNiCu-LDH is UV and visible light-responsive. Moreover, the introduction of Cu led to the narrow bandgap of CoNiCu-LDH (2.42 eV), compared with CoNi-LDH (2.69 eV). As a result, defect-rich CoNiCu-LDH could more efficiently harvest solar energy for the degradation of CECs molecules. Moreover, the higher photoelectrochemical efficiency and a longer excited-state lifetime of CoNiCu-LDH NFs were confirmed by using transient photocurrent measurements under chopped-light illumination (Fig. 5c) and time-resolved PL spectroscopy measurements (Fig. 5d). The results indicated that the newly developed CoNiCu-LDH is more favorable for electron-hole separation. Furthermore, the free-electron spin resonance (ESR) spin-trapping experiments indicated that hydroxyl radicals (•OH) and holes could increase after Cu introduction (Fig. 5e), while the characteristic peaks of DMPO- $O_2^{\bullet-}$ can be neglected, suggesting the •OH is the main active species. After calculation of valence band (VB) (Fig. S16), we found the VB hole to be positive to oxidize the OH^- to •OH (+1.99 eV), while the electrons on CB is incapable of reducing O_2 to $O_2^{\bullet-}$ (−0.33 eV) (Fig. 5f), being consistent with ESR results. Thus, the •OH is the main reactive species for catalytic degradation of the CECs. As a result, the CoNiCu-LDH NFs can be regenerated

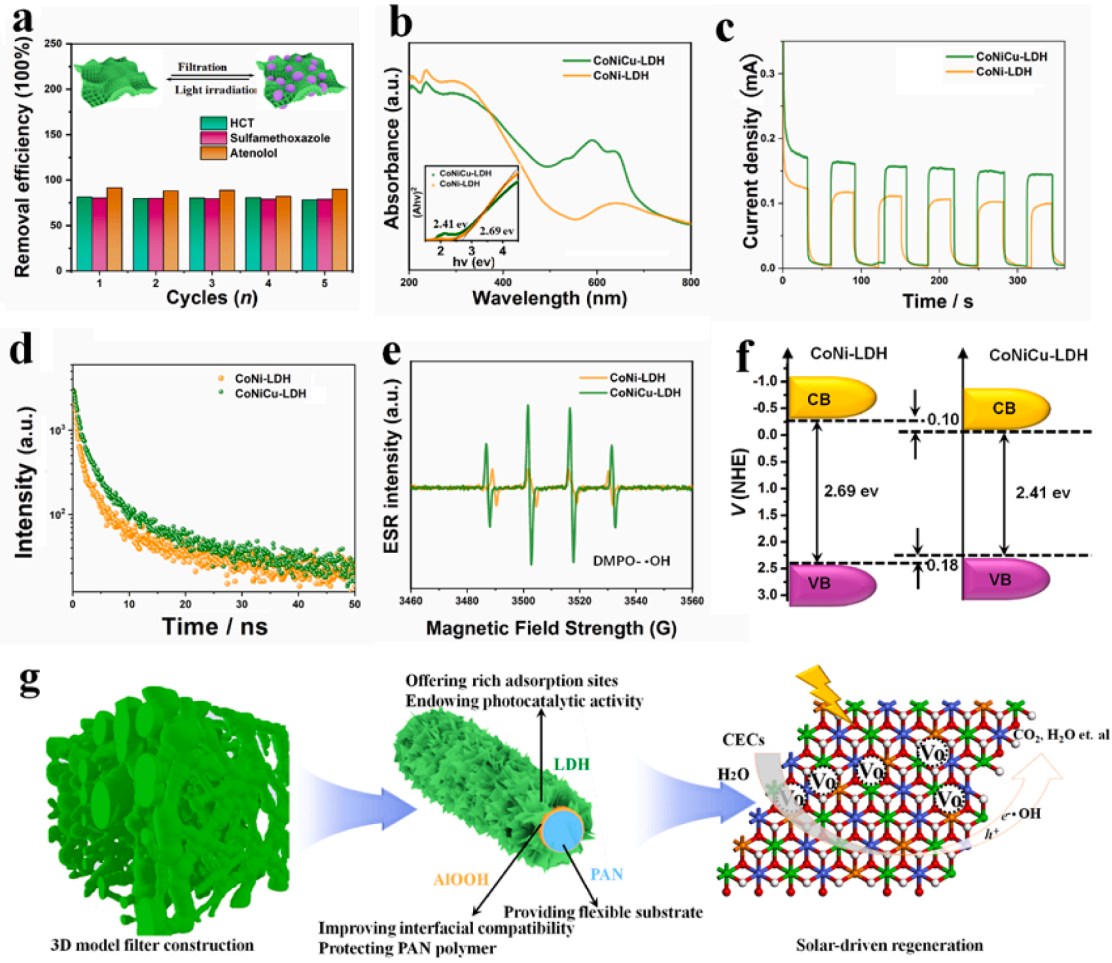

Fig. 5. (a) The regeneration performance of CoNiCu-LDH filter by the cycle of filtration and light irradiation. (b) UV–vis diffuse reflectance spectra and calculated bandgap (inset), (c) amperometric *I–t* curves at a potential of 0.6 V under chopped-light illumination ($\lambda > 200$ nm), (d) time-resolved PL decay profiles, (e) ESR spectra of radical adducts trapped to determine •OH radical by DMPO under light irradiation and (f) the band alignment for CoNi-LDH and CoNiCu-LDH. (g) The summary and highlights of LDHs filter with high adsorption capacity, fast removal rate and facile regeneration function for wastewater filtration.

for repeated filtration processes and removal of various contaminations in wastewater treatment. Thus, we developed a general strategy of designing defect-rich LDH-based microscopic adsorbent, shaping LDH adsorbent into mesoscopic NFs, and constructing a macroscopic 3D filter with photocatalytic driven regeneration function (Fig. 5g).

3. Conclusion

In summary, we have presented a systematic bottom-up methodology for constructing a fibrous adsorbent filter. A defect-rich CoNiCu-LDH with honeycomb-like morphology was grown on the flexible NFs and subsequently structured into 3D filters and this approach can be used to design various adsorbents based 3D filters. Specifically, this efficient strategy enables creating Vo and unsaturated metal sites on LDH to enrich active adsorption sites, which played an active role in the effective adsorption of CECs. In addition, the absorbent growth on the flexible NFs is favourable for combining a high density of active sites with mass transfer filtration. Based on our developed methodology for 3D modelling simulation of NFs filtration, a phenomenological equation was proposed to illustrate the combined effect of particle-fiber friction and chemical interaction on the filtration efficiency of CECs. The simulations combined with the experimental results reveal the synergetic effects of the active LDH adsorption sites and the particle-fiber friction between the LDH NFs and adsorbate molecules. Finally, we demonstrated light-driven regeneration of the LDH filter based on photocatalytic activity. Therefore, this work not only presents a novel defect-rich LDH adsorbent with dual functionality (adsorption and photocatalytic activity) but also provides a pathway to structure such inorganic adsorbents into 3D filters to facilitate the water treatment process.

4. Experimental section

4.1. Fabrication of LDH NFs

Firstly, the Co-ZIF-L growth on AlOOH coated PAN NFs was fabricated (See detail in Supporting Information on electrospinning PAN, dip coating AlOOH and in-situ growth of Co-ZIF-L). The LDH NFs were fabricated *via* the ion exchange method. Typically, 0.3 g of Ni $(NO_3)_2{\cdot}6H_2O$ and 0.05 g $Cu(NO_3)_2{\cdot}3H_2O$ was dissolved into the 100 ml ethanol and 5 ml water. Then the ZIF-L NFs mat (size: 10 cm × 10 cm) was immersed into the above solution. After reacting for 1 h at RT, the ZIF-L NFs was converted into CoNiCu-LDH NFs. To prove the introduction of $Cu^{\delta+}$ sites on LDH is helpful to improve the absorption and filtration efficiency, the control sample of CoNi-LDH NFs was also fabricated by using $Ni(NO_3)_2{\cdot}6H_2O$ reacting with ZIF-L NFs. The fabrication of other control adsorbents NFs and materials characterizations can be found in Supporting Information.

4.2. Kinetic adsorption measurements

The adsorption measurement was carried out at RT. Typically, 0.1 g of NFs (mass fraction of LDH is 12–15%) was added to 50 ml of CECs solution (100 mg L^{-1}). Analytical samples were extracted at pre-set time intervals and without centrifugation. The concentration of the CECs was measured on the basis of the maximum adsorption peak by using a UV/Vis spectrophotometer.

4.3. 3D fiber and model construction, filtration evaluation and simulation

The LDH NFs based 3D filter was fabricated by the following steps. Typically, the LDH NFs was cut into a round pie shape (diameter 1 cm) with a similar inner diameter of filter pipe. Then, the round pie-shaped LDH NFs were layer-by-layer stacked in filter pipe and further compressed the NFs to obtain the dense 3D fibrous filter with a thickness of 0.25 cm and 0.1 g (The stack layer number is around 18–20). Owing to the different structure of various adsorbent filter, we can not fix the same pressure to stack the individual layers if the thickness and weight was fixed in advance. The concentration of the filtered solution was measured on the basis of the adsorption peak by using a UV/Vis spectrophotometer. The detail on building a 3D model and simulating the filtration can be found in Supporting Information.

4.4. Regeneration investigation of LDH filter by light irradiation

Typically, the used wet CoNiCu-LDH filter was removed from the filter pipe and transferred to the sealed silica glass container. The used CoNiCu-LDH filter was irradiated by a 300 W Xe lamp as a light source ($\lambda > 200$ nm). After 1 h of irradiation, the CoNiCu-LDH filter was reloaded in the filter pipe for re-utilization. The regeneration experiment of CoNiCu-LDH filter can be conducted by cycling filtration and light irradiation operation. To further confirm the photocatalytic decomposition capability of pollutants for CoNiCu-LDH NFs. The experiments were performed at RT as follows: 0.1 g of used CoNiCu-LDH NFs was added to a 50 ml of CECs such as HCT, atenolol, and sulfamethoxazole (10 mg L^{-1}). Before light irradiation, the solution was stirred for 30 min in the dark to further exclude the adsorption interference, although the adsorption–desorption equilibrium between CECs solutions and the used CoNiCu-LDH NFs has been achieved. Then the solution was exposed to light irradiation, and the concentration of three CECs was detected by a UV/Vis spectrophotometer during the photocatalysis process.

Declaration of Competing Interest

The authors declare that they have no known competing financial interests or personal relationships that could have appeared to influence the work reported in this paper.

Acknowledgements

This work was supported by the Novo Nodisk Fundation (NNF18OC0034918) and the Danish Research Council (Grant No. 8022-00237B).

Appendix A. Supplementary data

Supplementary data to this article can be found online at https://doi.org/10.1016/j.cej.2021.132842.

References

[1] P. Verlicchi, M. Al Aukidy, E. Zambello, Occurrence of pharmaceutical compounds in urban wastewater: removal, mass load and environmental risk after a secondary treatment-a review, Sci. Total Environ. 429 (2012) 123–155.
[2] C. Gadipelly, A. Pérez-González, G.D. Yadav, I. Ortiz, R. Ibáñez, V.K. Rathod, K. V. Marathe, Pharmaceutical industry wastewater: review of the technologies for water treatment and reuse, Ind. Eng. Chem. Res. 53 (2014) 11571–11592.
[3] M. Patel, R. Kumar, K. Kishor, T. Mlsna, C.U. Pittman, D. Mohan, Pharmaceuticals of emerging concern in aquatic systems: chemistry, occurrence, effects, and removal methods, Chem. Rev. 119 (2019) 3510–3673.
[4] Y. Li, G. Zhu, W.J. Ng, S.K. Tan, A review on removing pharmaceutical contaminants from wastewater by constructed wetlands: design, performance and mechanism, Sci. Total Environ. 468-469 (2014) 908–932.
[5] B. Tiwari, B. Sellamuthu, Y. Ouarda, P. Drogui, R.D. Tyagi, G. Buelna, Review on fate and mechanism of removal of pharmaceutical pollutants from wastewater using biological approach, Bioresour. Technol. 224 (2017) 1–12.
[6] H. Waseem, M.R. Williams, R.D. Stedtfeld, S.A. Hashsham, Antimicrobial resistance in the environment, Water Environ. Res. 89 (10) (2017) 921–941.
[7] (a) Y. Shen, R. Yang, Y. Liao, J. Ma, H. Mao, S. Zhao, Tannin modified aminated silica as effective absorbents for removal of light rare earth ions in aqueous solution, Desalination and Water Treatment. 57 (2015) 1–8. (b) Y. Shen, S. Zhao, Y. Li, Q. Liu, C. Ma, H. Mao, Y. Liao, J. Ma, A feasible approach to dispose of soil washing wastes: adsorptive removal of chlorobenzene compounds in aqueous solutions using humic acid modified with monoolein (HA–M), RSC Adv. 7 (2017) 9662–9668. (c) L. Wang, C. Shi, L. Pan, X. Zhang, J.J. Zou, Rational design, synthesis, adsorption principles and applications of metal oxide adsorbents: A review, Nanoscale. 12 (2020) 4790–4815.

[8] Y. Peng, H. Huang, Y. Zhang, C. Kang, S. Chen, L. Song, D. Liu, C. Zhong, A versatile MOF-based trap for heavy metal ion capture and dispersion, Nat. Commun. 9 (2018) 187.
[9] (a) X Qiu, Y Shen, R Yang, H Zhang, S Zhao, Adsorption of RE^{3+} from aqueous solutions by bayberry tannin immobilized on chitosan, Environmental Technology. 40(2019) 202–209. (b) J.Z. Weng, S.Y. Wang, P.X. Zhang, C.P. Li, G. Wang, A review of metal-organic framework-derived carbon electrode materials for capacitive deionization, New Carbon Materials. 36 (2021) 117–132. (c) S. Xie, S. Wu, S. Bao, Y. Wang, Y. Zheng, D. Deng, L. Huang, L. Zhang, M. Lee, Z. Huang, Intelligent mesoporous materials for selective adsorption and mechanical release of organic pollutants from water, Adv. Mater. 30 (2018) 1–5.
[10] L. Ji, F. Liu, Z. Xu, S. Zheng, D. Zhu, Adsorption of pharmaceutical antibiotics on template-synthesized ordered micro- and mesoporous carbons, Environ. Sci. Technol. 44 (2010) 3116–3122.
[11] J. Jiang, R. Babarao, Z. Hu, Molecular simulations for energy, environmental and pharmaceutical applications of nanoporous materials: from zeolites, metal–organic frameworks to protein crystals, Chem. Soc. Rev. 40 (2011) 3599–3612.
[12] M. Momina, S. Shahadat, Isamil, Regeneration performance of clay-based adsorbents for the removal of industrial dyes: A review, RSC Adv. 8 (2018) 24571–24587.
[13] Y. Si, X. Wang, L. Dou, J. Yu, B. Ding, Ultralight and fire-resistant ceramic nanofibrous aerogels with temperature-invariant superelasticity, Sci. Adv. 4 (2018) 8925.
[14] Y. Lan, X. Han, M. Tong, H. Huang, Q. Yang, D. Liu, X. Zhao, C. Zhong, Materials genomics methods for high-throughput construction of COFs and targeted synthesis, Nat. Commun. 9 (2018) 1–10.
[15] Y. Dou, W. Zhang, A. Kaiser, Electrospinning of metal–organic frameworks for energy and environmental applications, Adv. Sci. 7 (2020) 1902590.
[16] A.X. Lu, M. McEntee, M.A. Browe, M.G. Hall, J.B. Decoste, G.W. Peterson, MOFabric: electrospun nanofiber mats from PVDF/UiO-66-NH_2 for chemical protection and decontamination, ACS Appl. Mater. Interfaces. 9 (2017) 13632–13636.
[17] D.L. McCarthy, J. Liu, D.B. Dwyer, J.L. Troiano, S.M. Boyer, J.B. Decoste, W. E. Bernier, W.E. Jones, Electrospun metal-organic framework polymer composites for the catalytic degradation of methyl paraoxon, New J. Chem. 41 (2017) 8748–8753.
[18] Q. Wang, D. Ohare, Recent advances in the synthesis and application of layered double hydroxide (LDH) nanosheets, Chem. Rev. 112 (2012) 4124–4155.
[19] L. Ma, Q. Wang, S.M. Islam, Y. Liu, S. Ma, M.G. Kanatzidis, Highly selective and efficient removal of heavy metals by layered double hydroxide intercalated with the MoS_4^{2-} ion, J. Am. Chem. Soc. 138 (2016) 2858–2866.
[20] Y. Zou, X. Wang, Y. Ai, Y. Liu, J. Li, Y. Ji, X. Wang, Coagulation behavior of graphene oxide on nanocrystallined Mg/Al layered double hydroxides: batch experimental and theoretical calculation study, Environ. Sci. Technol. 50 (2016) 3658–3667.
[21] M. Zubair, M. Daud, G. McKay, F. Shehzad, M.A. Al-Harthi, Recent progress in layered double hydroxides (LDH)-containing hybrids as adsorbents for water remediation, Appl. Clay Sci. 143 (2017) 279–292.
[22] C. Li, S. Zhao, X. Yao, L. He, S. Xu, X. Shen, Z. Yao, The catalytic mechanism of intercalated chlorine anions as active basic sites in MgAl-layered double hydroxide for carbonyl sulfide hydrolysis, Environ. Sci. Pollut. Res. (2021), https://doi.org/10.1007/s11356-021-16204-3.
[23] Y. Dou, S. Xu, X. Liu, J. Han, H. Yan, M. Wei, D.G. Evans, X. Duan, Transparent, flexible films based on layered double hydroxide/cellulose acetate with excellent oxygen barrier property, Adv. Funct. Mater. 24 (2014) 514–521.
[24] Y. Zhao, Y. Zhao, G.I.N. Waterhouse, L. Zheng, X. Cao, F. Teng, L.Z. Wu, C.H. Tung, D. O'Hare, T. Zhang, Layered-double-hydroxide nanosheets as efficient visible-light-driven photocatalysts for dinitrogen fixation, Adv. Mater. 29 (2017) 1–10.
[25] S. Kim, J. Fahel, P. Durand, E. André, C. Carteret, Ternary layered double hydroxides (LDHs) based on Co-, Cu-substituted ZnAl for the design of efficient photocatalysts, Eur. J. Inorg. Chem. 2017 (2017) 669–678.
[26] D. Ji, L. Fan, L. Tao, Y. Sun, M. Li, G. Yang, T.Q. Tran, S. Ramakrishna, S. Guo, The kirkendall effect for engineering oxygen vacancy of hollow Co_3O_4 nanoparticles toward high-performance portable zinc–air batteries, Angew. Chemie - Int. Ed. 58 (2019) 13840–13844.
[27] L. Lu, J. Li, D.H.L. Ng, P. Yang, P. Song, M. Zuo, Synthesis of novel hierarchically porous Fe_3O_4@MgAl–LDH magnetic microspheres and its superb adsorption properties of dye from water, J. Ind. Eng. Chem. 46 (2017) 315–323.
[28] C. Lei, M. Pi, P. Kuang, Y. Guo, F. Zhang, Organic dye removal from aqueous solutions by hierarchical calcined Ni-Fe layered double hydroxide: Isotherm, kinetic and mechanism studies, J. Colloid Interface Sci. 496 (2017) 158–166.
[29] X. Liu, C. Wang, Y. Dou, A. Zhou, T. Pan, J. Han, M. Wei, A NiAl layered double hydroxide@carbon nanoparticles hybrid electrode for high-performance asymmetric supercapacitors, J. Mater. Chem. A. 2 (2014) 1682–1685.
[30] Y. Dou, S. Zhang, T. Pan, S. Xu, A. Zhou, M. Pu, H. Yan, J. Han, M. Wei, D.G. Evans, X. Duan, TiO_2@layered double hydroxide core-shell nanospheres with largely enhanced photocatalytic activity toward O_2 generation, Adv. Funct. Mater. 25 (2015) 2243–2249.
[31] W. Sambaer, M. Zatloukal, D. Kimmer, 3D air filtration modeling for nanofiber based filters in the ultrafine particle size range, Chem. Eng. Sci. 82 (2012) 299–311.
[32] W. Sambaer, M. Zatloukal, D. Kimmer, 3D modeling of filtration process via polyurethane nanofiber based nonwoven filters prepared by electrospinning process, Chem. Eng. Sci. 66 (2011) 613–623.
[33] R.B. Bird, W.E. Stewart, E.N. Lightfoot, c2007, Transport phenomena. 2nd, rev. ed. New York: J. Wiley.
[34] Y. Chen, Z. Fan, Z. Zhang, W. Niu, C. Li, N. Yang, B. Chen, H. Zhang, Two-dimensional metal nanomaterials: synthesis, properties, and applications, Chem. Rev. 118 (2018) 6409–6455.
[35] M. Ding, R.W. Flaig, H.L. Jiang, O.M. Yaghi, Carbon capture and conversion using metal-organic frameworks and MOF-based materials, Chem. Soc. Rev. 48 (2019) 2783–2828.
[36] Y. Lee, J.H. Choi, H.J. Jeon, K.M. Choi, J.W. Lee, J.K. Kang, Titanium-embedded layered double hydroxides as highly efficient water oxidation photocatalysts under visible light, Energy Environ. Sci. 4 (2011) 914–920.
[37] X. Chang, T. Wang, J. Gong, CO_2 photo-reduction: Insights into CO_2 activation and reaction on surfaces of photocatalysts, Energy Environ. Sci. 9 (2016) 2177–2196.
[38] C. Zhao, Z. Chen, R. Shi, X. Yang, T. Zhang, Recent advances in conjugated polymers for visible-light-driven water splitting, Adv. Mater. 32 (2020) 1–52.